CHAPTER 10
FORMATION OF AN INVARIANT TARGET POSITION MAP

10.1. Invariant Self-Regulating Multimodal Maps

In Section 1.4, we described properties that it would be desirable for a target position map (TPM) to possess. The most important property is that of map *invariance*; namely, the many-to-one activation of a single spatial locus that corresponds to a prescribed target position, no matter which of the many possible combinations of retinal position and eye position give rise to that target position. In an invariant TPM, after movements of the eye occur with respect to a fixed light source, no change occurs in the spatial locus which the light activates. More generally, if an invariant TPM stores a pattern of n lights, no change occurs in the spatial positions of map activation as the eyes inspect the successive lights. Although the spatial positions of map activation do not change, other more subtle indices may change. For example, habituation may reduce the activation of a target position if it is stored in the map for a long time (Grossberg, 1980, 1982b). Such an habituated target position could gradually lose its ability to attract an observer's attention.

In a noninvariant TPM, by contrast, a different map position is activated by a fixed light each time the observer moves his eyes. A single light can hereby activate a series of target positions. These target loci cannot habituate as a function of the total time that the light has been stored. Using multiple noninvariant encodings of a single target position in a predictive command network (PCN) could cause serious problems, since the very act of saccading to a target position could activate a new spatial locus corresponding to that target position, as well as new loci corresponding to all the remaining target positions, simply because the eyes moved. These multiple activations and reactivations could cause a breakdown in the temporal order code that was moving the eyes (Chapter 9). We therefore restrict our attention to the design of invariant TPMs in this chapter.

As in our discussion of spatial maps in Chapter 6, we will describe more than one possible design of an invariant TPM. Both designs satisfy the theory's functional requirements and both are built up from plausible neural mechanisms. One TPM design depends more heavily on prewired mechanisms. The other design is built up through learning. This latter design has remarkable formal properties. Indeed, it possesses all of the properties which were listed in Section 1.4 as desirable ones for a TPM to have, including invariance, self-regulation, error tolerance, and multimodal self-consistency. Of special interest is the way in which macroscopic functional properties emerge from the interaction of microscopic cellular processes. Notable among the microscopic processes from which an invariant TPM can be synthesized are chemical transmitter systems that possess autoreceptors. Certain catecholaminergic transmitter systems are

well known to possess autoreceptors (Cubeddu, Hoffmann, and James, 1983; Dubocovich and Weiner, 1982; Groves and Tepper, 1983; Groves, Fenster, Tepper, Nakamura, and Young, 1981; Niedzwiecki, Mailman, and Cubeddu, 1984; Siever and Sulser, 1984; Tepper, Young, and Groves, 1984). However, this is the first time that they have been used to explain such a high-order functional capability as invariant multimodal map formation. We will show how to combine a known transmitter learning equation and transmitter autoreceptor equation (Grossberg, 1981, 1984) into a new self-regulating transmitter learning equation. When this new transmitter learning equation is obeyed at all the learning synapses of a properly designed neural circuit, it enables the circuit as a whole to learn an invariant TPM. In particular, the autoreceptive part of the new learning equation enables the circuit as a whole to compensate for variable numbers of sampling sources without causing any contradictions in the rules which emerge through learning. This theory of how invariant multimodal maps can self-organize is potentially relevant to a large class of problems concerning the emergence of maps and rules in neurobiology and artificial intelligence.

10.2. Prewired Positional Gradients: The Mean Value Property

Several schemes for generating prewired TPMs are known. They are all based on variants of the following simple idea. Consider for the moment one-dimensional maps; for example, maps of target position in a horizontal direction. Imagine that a one-dimensional retinotopic map (RM) and a one-dimensional eye position map (EPM) map topographically onto a one-dimensional TPM, as in Figure 10.1. Denote the activated position of the RM by R and the activated position of the EPM by E. Our task is to design an TPM which is maximally excited at a single spatial locus, in response to any physical choice of R and E such that $R + E =$ constant. Denote the one-dimensional spatial variable of the TPM by p. We will describe several schemes which imply that the maximally excited spatial locus of the TPM is

$$p = \frac{1}{2}(R + E); \tag{10.1}$$

that is, the mean value of R and E.

The formal constraints governing schemes of this type are easily described. Their neural instantiation is another matter. For example, suppose that activation of position R in the RM causes a spatially distributed input to the TPM of size

$$I_R(p) = Ae^{-\mu(R-p)^2} \tag{10.2}$$

and that activation of position E in the EPM causes a spatially distributed input to the TPM of size

$$I_E(p) = Be^{-\mu(E-p)^2} \tag{10.3}$$

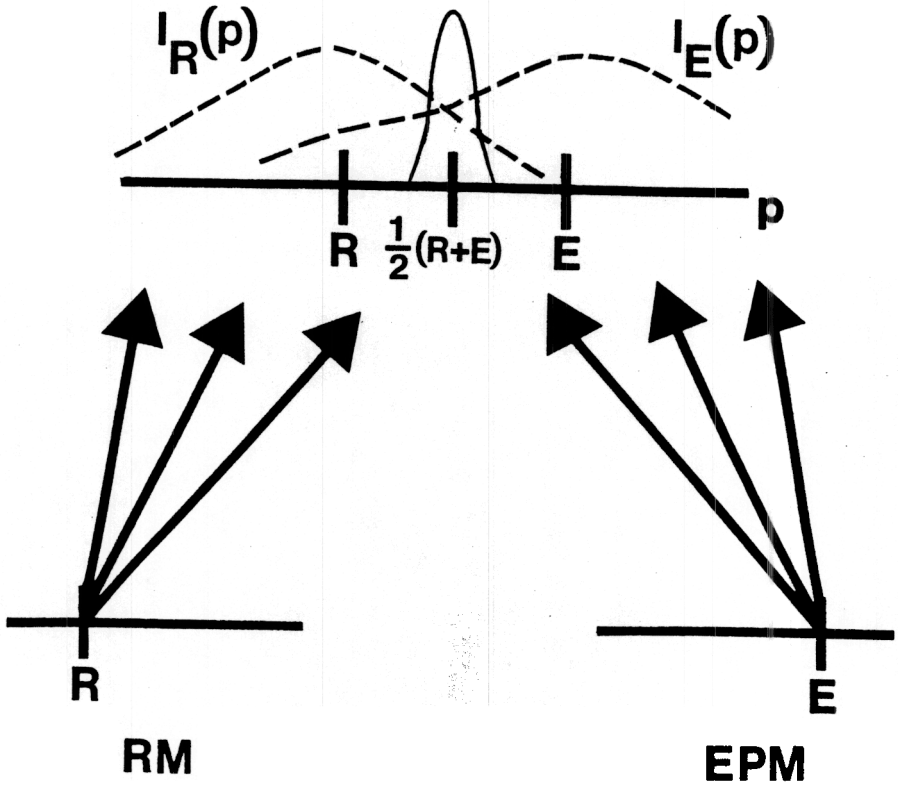

Figure 10.1. Generating a 1-dimensional target position map (TPM) from a 1-dimensional retinotopic map (RM) and eye position map (EPM): Each position R in the RM and E in the EPM activates a broadly distributed gradient of pathways to the TPM. The TPM contrast enhances the total inputs, thereby focusing its activity near position $\frac{1}{2}(R + E)$.

In other words, the RM and the EPM cause Gaussianly distributed inputs to the TPM whose maxima occur at positions $p = R$ and $p = E$, respectively. Such gradients could develop, for example, due to growth of connections from the RM and EPM to the TPM guided by TPM morphogens which undergo significant lateral diffusion within the TPM.

Suppose that the activity pattern caused within the TPM by active R and E loci is given by

$$x_1(p) = I_R(p)I_E(p). \tag{10.4}$$

Alternatively, suppose that the TPM activity pattern is defined by

$$x_2(p) = I_R(p) + I_E(p). \tag{10.5}$$

In other words, the input patterns generate TPM activation either through a multiplicative (shunting, gating) process, as in (10.4), or through an additive process, as in (10.5). The shunting process is more robust, but both processes work within an achievable parameter range.

In the shunting case, equations (10.2)–(10.4) imply that

$$x_1(p) = ABe^{-\mu[(R-p)^2+(E-p)^2]} \tag{10.6}$$

The position $p = P_1$ at which $x_1(p)$ is maximum is found by minimizing quantity

$$(R-p)^2 + (E-p)^2. \tag{10.7}$$

This minimum occurs at

$$P_1 = \frac{1}{2}(R+E). \tag{10.8}$$

A similar conclusion holds for the additive gradient $x_2(p)$. An important addition constraint holds in the additive case, however, since a maximum occurs at

$$P_2 = \frac{1}{2}(R+E) \tag{10.9}$$

only if the positions R and E are not too far apart relative to the decay rate μ of the Gaussian positional gradients. In particular $y = \mid R - E \mid$ must not be larger than the unique positive root of the equation

$$2e^{-\frac{\mu}{4}y^2} - e^{-\mu y^2} = 1. \tag{10.10}$$

Thus broad positional gradients are needed to admit a wide range of R and E values. No such quantitative constraints on μ exist in the shunting case. However, even in the shunting case, μ must be chosen sufficiently small to guarantee physically realizable gradients which cover the entire TPM.

Gaussian gradients are not the only ones that imply the mean value property in (10.8) and (10.9). Exponential gradients $I_R(p) = Ae^{-\mu|R-p|}$ and $I_E(p) = Be^{-\mu|E-p|}$ could, for example, also be used, as could other gradients that decrease with the distance from the inducing input sources R and E.

Invariant target positions can also be derived from two dimensional RMs and EPMs. Then formulas like (10.2) and (10.3) for $R(p)$ and $E(p)$, respectively, generalize to

$$I_R(p,q) = (A_1 e^{-\mu(R_1-p)^2}, A_2 e^{-\nu(R_2-q)^2}) \tag{10.11}$$

and

$$I_E(p,q) = (B_1 e^{-\mu(E_1-p)^2}, B_2 e^{-\nu(E_2-q)^2}) \tag{10.12}$$

and a formula such as (10.4) for $x_1(p)$ generalizes to

$$x_1(p,q) = (A_1 B_1 e^{-\mu[(R_1-p)^2+(E_1-p)^2]}, A_2 B_2 e^{-\nu[(R_2-q)^2+(E_2-q)^2]}). \tag{10.13}$$

The spatial locus of maximal activity of the activity pattern $x_1(p,q)$ occurs at the position (P_1, Q_1) such that

$$P_1 = \frac{1}{2}(R_1 + E_1) \tag{10.14}$$

and

$$Q_1 = \frac{1}{2}(R_2 + E_2). \tag{10.15}$$

In both the one-dimensional and two-dimensional maps, the strongest input constraint is the requirement that eye positions match up, at least approximately, with the corresponding retinal positions. This requirement can be met, for example, by mapping tonic cell output patterns into an EPM using a one-dimensional or three-dimensional position-threshold-slope (PTS) shift map (Chapter 6.3).

If retinal position and eye position are combined one dimension at a time, then an extra processing stage is needed to combine the one-dimensional maps. This final stage only needs to achieve response selectivity, because invariance is already guaranteed by the one-dimensional maps. Several types of coincidence detectors can achieve the desired selectivity, as can an adaptive filter (Chapter 6).

In all versions of a prewired TPM, the final stage must contrast enhance the final activity pattern in order to convert its diffusely distributed activity into a sharply defined target position. In general, many of the mechanisms that go into the design of prewired TPMs are specializations of the general spatial mapping mechanisms that were described in Chapter 6.

It remains to discuss how shunting rules like (10.4) and additive rules like (10.5) could be physically instantiated. The additive rule (10.5) has an obvious neural interpretation. The shunting rule (10.4) deserves serious consideration if only because preliminary data of Anderson, Essick, and Siegel (1984) suggest that the interaction of eye position and retinal position information in the parietal cortex of macaque monkeys may be approximately multiplicative. A presynaptic gating action of EPM synaptic knobs on RM synaptic knobs is a possible shunting mechanism.

10.3. Self-Organizing Target Position Maps: Multimodal Sampling of a Unimodal Eye Position Map

We now turn to a problem that we find much more engaging: the problem of invariant TPM self-organization. In our treatment of this problem, we will assume that an RM and an EPM exist and act as sources of conditionable pathways which converge upon another EPM. Denote the sampling EPM by EPM_1 and the sampled EPM by EPM_2. We will show how cooperative self-organization of the signalling from the RM and the EPM_1 convert EPM_2 into an invariant TPM. The internal structures of the sampling maps RM and EPM_1 do not need to be topographically organized, but EPM_2 does have an internal topography. Moreover, the design works given any number of sampling maps, not just two. Any number of modalities can join to learn a globally self-consistent rule at the sampled map using the mechanisms that we will describe. We focus on the case of two sampling maps RM and EPM_1 because that is our main application.

Suppose that the RM and the EPM_1 store a retinal position and an initial eye position in short term memory (STM) before a saccade begins. Assume that STM storage persists until after the saccade is over. Also assume that the accuracy of the saccades progressively improves through time due to learning via second light error signals (Chapter 3). In other words, the saccades in question are the visually reactive saccades of the retinotopic command network (RCN). The invariant TPM that we will describe is built up on the shoulders of RCN learning.

We will consider a time frame when these RCN-generated saccades are already quite accurate. After such an accurate saccade terminates, a Now Print gate opens, just like in the HMI (Chapter 9), and allows the RM and the EPM_1 to sample the activity locus within the EPM_2. This EPM_2 activity locus encodes target position *because* the saccade was accurate. It codes target position *invariantly* because it is a unimodal code that is directly derived from final eye position, rather than from a multimodal combination of retinal position and initial eye position.

This kind of many-to-one learning will go on until activating positions within the RM and the EPM_1 can begin to reliably activate EPM_2 positions before a saccade occurs. Once the RM and the EPM_1 can reliably activate the EPM_2, then the EPM_2 will automatically become an invariant TPM.

Then the invariant TPM positions can begin to learn TPM muscle coordinates at the HMI, the HMI vectors can begin to be encoded by an RM, and so on, as in Chapters 4 and 9. Processing stages that learn temporally stable maps can successively support the formation of further temporally stable maps. Thus, intentional movement controls emerge in a developmental progression.

10.4. Double Duty by Sampling Maps and their Neural Interpretation

The retinotopic map RM that samples EPM_2 has the same properties as the RM which is the basis of retinotopic sampling of the adaptive gain (AG) stage in the RCN (Chapter 3). The simplest hypothesis is that these two maps are really the same map, and thus that this RM also controls the direct unconditioned pathway and the indirect conditioned pathway that generate visually reactive saccades. The eye position map EPM_1 that samples the EPM_2 has the same properties as the EPM that updates eye position signals to the SG within the eye position update network, or EPUN (Chapter 7). The simplest hypothesis is that these two maps are also a single map. We therefore interpret EPM_1 as the movement EPM, or EPM_M, that was discussed in Chapter 9.

The sampled map EPM_2 becomes an invariant TPM by virtue of the learning rules whereby RM and EPM_1 interact with it. The map EPM_2 need not have any internally invariant properties. Any reasonably continuous change of activation locus in EPM_2 with final eye position will do. Any of the spatial mapping mechanisms of Chapter 6 satisfy this modest formal requirement. The theory thus suggests that the invariant TPM emerges from a noninvariant EPM.

The posterior parietal cortex is the most likely anatomical site for such an invariant TPM (Hyvärinen, 1982; Lynch, 1980; Motter and Mountcastle, 1981). Hence the model suggests that, at an early developmental stage, the posterior parietal cortex may be sensitive to a unimodal source of final eye position before its cells can encode target position as a function of multimodal visual and initial eye position signals. The model also suggests that the RM and the EPM_1 which sample EPM_2 are no "higher" in the cortical hierarchy than the parietal cortex.

Given this constraint, the RM is best interpreted at the present time as being somewhere on the pathways from superior colliculus and visual cortex to posterior parietal lobe. The EPM_1, and thus the movement EPM, or EPM_M of Section 9.9 may be housed in the parietal cortex, since it is probably not found in visual cortex. This argument makes it seem unlikely that the EPM_M lies in the frontal cortex, where the postural EPM, or EPM_{Pos}, seems to reside. Such an anatomical interpretation of the EPM_M suggests that many cells in parietal cortex are exclusively sensitive to eye position, as opposed to light, even in the adult, and that these cells will be activated by initial eye position rather than by final eye position.

10.5. Associative Learning at Autoreceptive Synaptic Knobs

The learning rule which we will apply joins together two properties of chemical transmitter models (Grossberg, 1981, 1984) into a new self-regulating transmitter learning equation. One property concerns an associative learning rule of the form

$$\frac{d}{dt}z_{ij} \quad \epsilon S_i[-Az_{ij} + Bx_j] \tag{10.16}$$

In (10.16), z_{ij} is interpreted as the production rate of a chemical transmitter in the synaptic knob(s) of pathway(s) e_{ij} from cell (population) v_i to cell (population) v_j. This is essentially the same learning rule that we used in (6.19) to learn a spatial map. In (10.16), S_i is a presynaptic sampling signal that travels along pathway e_{ij}. If $S_i = 0$, then $\frac{d}{dt}z_{ij} = 0$. Hence a presynaptic signal, rather than the postsynaptic signal of (6.19), turns on the plasticity of this transmitter system. The small parameter ϵ just says that the learning rate can be chosen to be slow even if S_i can become large.

As in our discussion of associative learning in Chapter 6, we also assume that transmitter is released at a rate proportional to $S_i z_{ij}$. This property leads us to consider the second property of chemical transmitter models that we will use. The equation

$$\frac{d}{dt}z_{ij} \quad C(D - z_{ij}) \quad S_i z_{ij} - E\sum_{k=1}^{n} S_k z_{kj} \tag{10.17}$$

says that, in the absence of any transmitter release (all $S_k = 0$), z_{ij} accumulates to a target level D. This target level is determined by two factors: a constant production rate (term CD) combined with feedback inhibition (term $-Cz_{ij}$) of transmitter z_{ij} onto an intermediate stage of transmitter production. When the sampling signal S_i is turned on, transmitter is released at a rate $S_i z_{ij}$; hence the term $-S_i z_{ij}$. The additional term $-E\sum_{k=1}^{n} S_k z_{kj}$ says that a fraction of the total transmitter released at cell v_j is reabsorbed by autoreceptors into the synaptic knobs of pathway e_{ij}. Once in these knobs, the reabsorbed transmitter inhibits transmitter production via feedback inhibition.

A major effect of autoreceptive inhibition is to normalize the total amount of transmitter impinging upon a postsynaptic cell. To see why this is so, suppose for definiteness that all presynaptic signals $S_i = 1$. Let the total amount of transmitter produced in pathways abutting v_j be denoted by $z_j = \sum_{k=1}^{n} z_{kj}$. Then (10.17) implies that

$$\frac{d}{dt}z_j = nCD - Cz_j \quad (1 + nE)z_j \tag{10.18}$$

At equilibrium, $\frac{d}{dt}z_j = 0$, so that

$$z_j = \frac{nCD}{1 + C + nE}. \tag{10.19}$$

By (10.19), $z_j \leq \frac{CD}{E}$ no matter how many pathways impinge upon v_j. Thus the total amount of transmitter does not grow with the total number of pathways. This is the normalization, or conservation, property that we seek.

In our present application, this type of normalization helps to achieve self-regulation of the TPM. In Grossberg (1981), this property was used to explain how very large lesions of the nigrostriatal bundle can cause surprisingly minor behavioral deficits (Stricker and Zigmond, 1976). To see how such sparing can occur in system (10.17), suppose that some pathways p_{ij} to v_j are cut. Then feedback inhibition of transmitter production within the remaining pathways is reduced, thereby amplifying their transmitter production levels in a compensatory fashion.

The transmitter learning rule that we will use combines the transmitter laws (10.16) and (10.17) into the single law

$$\frac{d}{dt}z_{ij} = eS_i[-Fz_{ij} + Gx_j - H\sum_{k=1}^{n} S_k z_{kj}]. \tag{10.20}$$

In (10.20), the constant asymptote D of (10.17) is replaced, due to learning, by a variable asymptote proportional to x_j, as in (10.16). This apparently simple change has profound consequences for the course of learning when equation (10.20) holds at all the cells v_j at which learning occurs. Term $-AS_iz_{ij}$ in (10.16) and term $-S_iz_{ij}$ in (10.17) are absorbed into term $-FS_iz_{ij}$ in (10.20). Term S_i in (10.20) also gates the autoreceptive influx $-H\sum_{k=1}^{n} S_k z_{kj}$. Although this property is of conceptual interest, it did not substantially influence our simulations due to the slow forgetting rate $-eF$.

Given the learning rule (10.20), all of the desired TPM properties arise through self-organization just so long as combinations of RM and EPM_1 positions are allowed to sample the correct target eye positions within EPM_2. Thus individual cells in the EPM_2 can receive simultaneous sampling signals from the RM and the EPM_1. By equation (10.20), an RM-activated LTM trace and an EPM_1-activated LTM trace can influence one another through autoreceptive interactions at the same sampled cell in EPM_2. We will now describe how this interaction influences the self-organization process both mathematically and through computer simulation results.

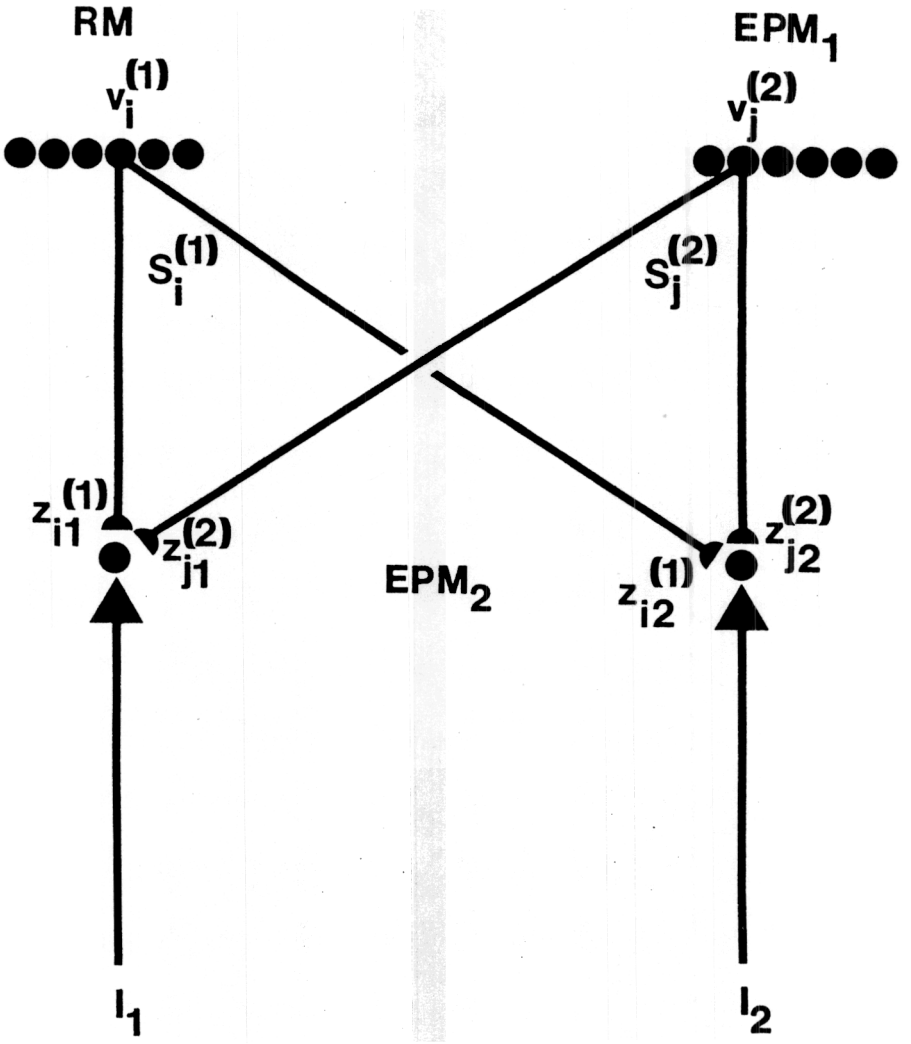

Figure 10.2. Self-organization of an invariant self-regulating target position map due to simultaneous sampling by a retinotopic map (RM) and an eye position map (EPM_1) of another eye position map (EPM_2): Pairs of sampling cells $v_i^{(1)}$ in RM and $v_j^{(2)}$ in EPM_1 conjointly learn the target position patterns (I_1, I_2) via their LTM traces $z_{ik}^{(1)}$ and $z_{jk}^{(2)}$, respectively, where $k = 1, 2$.

10.6. Multimodal Learning of Invariant Self-Regulating Spatial Maps

Figure 10.2 describes a model in which two fields RM and EPM_1 sample spatial patterns of activity across a field EPM_2. Field RM contains p cells $v_i^{(1)}$, $i = 1, 2, \ldots, p$, and field EPM_1 contains q cells $v_j^{(2)}$, $j = 1, 2, \ldots, q$. To simplify our graphic displays, we have chosen EPM_2 to contain only two cells V_1 and V_2, although the results go through for any number of cells, as Section 10.6 will illustrate. Denote the sampling signal from $v_i^{(1)}$ by $S_i^{(1)}$ and the sampling signal from $v_j^{(2)}$ by $S_j^{(2)}$. The LTM traces from $v_i^{(1)}$ to V_k are denoted by $z_{ik}^{(1)}$, and from $v_j^{(2)}$ to V_k are denoted by $z_{jk}^{(2)}$, $i = 1, 2, \ldots, p$; $j = 1, 2, \ldots, q$; $k = 1, 2$. The activities of V_1 and V_2 are denoted by x_1 and x_2, respectively. The inputs which activate V_1 and V_2 are denoted by I_1 and I_2, respectively. The input pattern (I_1, I_2) represents the target position that is sampled by an appropriate pair $v_i^{(1)}$ and $v_j^{(2)}$ of RM and EPM_1 cells, respectively. We will show how conjoint sampling by pairs of RM and EPM_1 cells leads to learning of this input pattern. Learning is not harmed by increasing the number of cells in RM and EPM_1, despite the fact that such an increase in cells also increases the number of cells in EPM_1 with which each cell in RM is paired, and conversely. Thus no contradictions in rule learning are generated by adding more cells. This example raises the possibility that RM and EPM_1 *in vivo* may directly learn a pattern of corollary discharges at the HMI rather than an invariant TPM.

The equations governing the model are as follows.

EPM_2 Activities

Let

$$\frac{d}{dt}x_1 = -x_1 + I_1 + z_1, \tag{10.21}$$

where z_1 equals the total sampling input from RM and EPM_1 to V_1, namely

$$z_1 = \sum_{i=1}^{p} S_i^{(1)} z_{i1}^{(1)} + \sum_{j=1}^{q} S_j^{(2)} z_{j1}^{(2)}. \tag{10.22}$$

Similarly, let

$$\frac{d}{dt}x_2 = -x_2 + I_2 + z_2, \tag{10.23}$$

where

$$z_2 = \sum_{i=1}^{p} S_i^{(1)} z_{i2}^{(1)} + \sum_{j=1}^{q} S_j^{(2)} z_{j2}^{(2)}. \tag{10.24}$$

Long Term Memory Traces

Let

$$\frac{d}{dt}z_{ik}^{(1)} = \epsilon S_i^{(1)}[-Fz_{ik}^{(1)} + Gx_k - Hz_k] \tag{10.25}$$

$$\frac{d}{dt}z_{jk}^{(2)} = \epsilon S_j^{(2)}[-Fz_{jk}^{(2)} + Gx_k - Hz_k] \tag{10.26}$$

where $i = 1, 2, \ldots, p$; $j = 1, 2, \ldots, q$; and $k = 1, 2$.

It remains to specify the rule whereby RM and EPM_1 signals can sample a consistent target position pattern across EPM_2. On every trial, one population $v_i^{(1)}$ in RM and one population $v_j^{(2)}$ in EPM_1 is randomly activated. We let $i = i_n$ be the randomly chosen index in $\{1, 2, \ldots, p\}$ of an RM cell and $j = j_n$ be the randomly chosen index in $\{1, 2, \ldots, q\}$ of an EPM_1 cell on trial n. In other words,

Sampling Signals

$$S_i^{(1)} = \begin{cases} 1 & \text{if } i = i_n \\ 0 & \text{if } i \neq i_n \end{cases} \tag{10.27}$$

$$S_j^{(2)} = \begin{cases} 1 & \text{if } j = j_n \\ 0 & \text{if } j \neq j_n, \end{cases} \tag{10.28}$$

where $n = 1, 2, \ldots, N$ and N is the number of learning trials. The inputs to V_1 and V_2 on trial n are denoted by (I_{1n}, I_{2n}). In order to represent target positions, the inputs are chosen to be a function of $i_n + j_n$. For definiteness we consider the following function.

Inputs

$$I_{1n} + I_{2n} = K \tag{10.29}$$

$$I_{2n} = L(i_n + j_n), \tag{10.30}$$

where K and L are positive constants. In other words, both I_{1n} and I_{2n} are linear functions of the total sampling index $i_n + j_n$, and I_{2n} increases as I_{1n} decreases.

Figure 10.3 describes how the LTM traces from RM and EPM_1 to EPM_2 build up as a function of how many cells in RM and EPM_1 are allowed to sample EPM_2. Each figure represents a superposition of RM and EPM_1 LTM values. In Figure 10.3b, only 40 cells in RM and EPM_1 sample EPM_2. In Figure 10.3d, the number of sampling cells in each field is increased to 80, and in Figure 10.3f to 160. Notice that increasing the number of cells, and hence the number of sampling combinations, in going from Figure 10.3b to 10.3d to 10.3f has no significant effect on the LTM values of the previous maps. In other words, the learning process is self-regulatory.

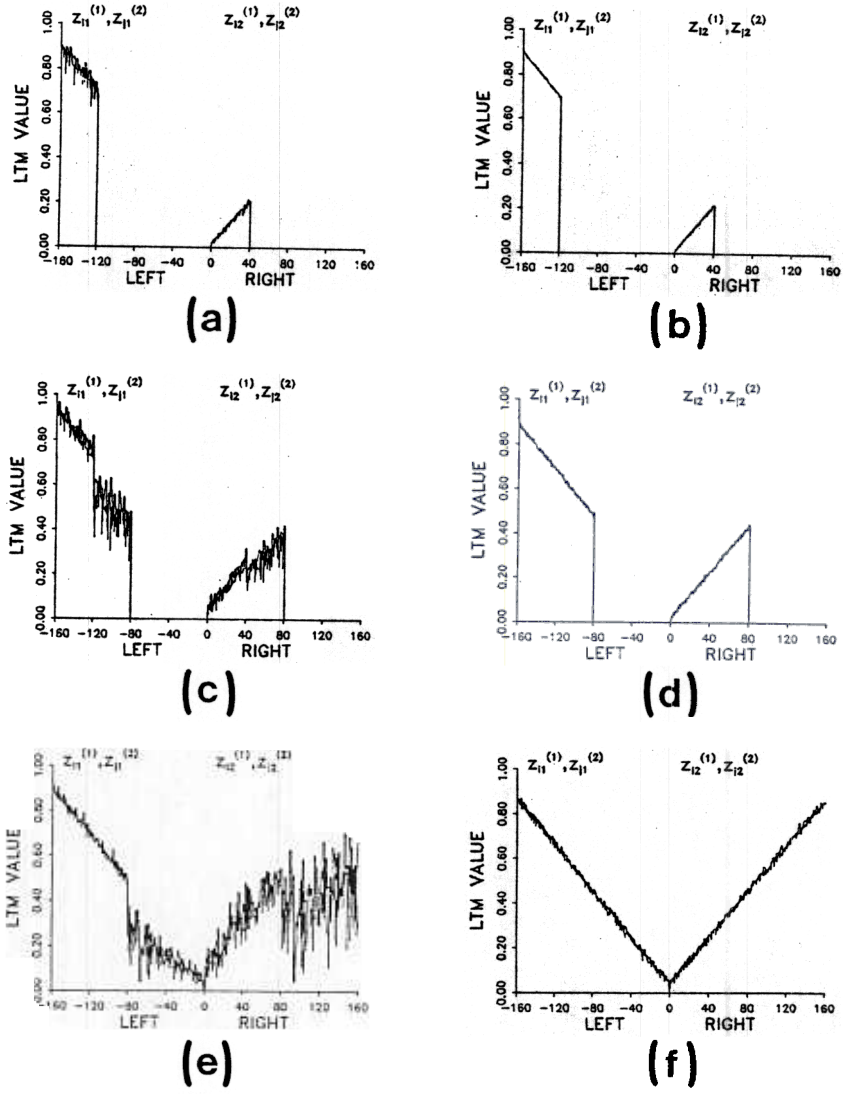

Figure 10.3. Expansion of LTM maps due to increase of the number of cells in the RM and the EPM_1 which sample the EPM_2: (a) Intermediate stage of learning using 40 sampling cells in the RM and the EPM_1; (b) Final stage of learning using 40 cells in each sampling field; (c) Intermediate stage of learning using 80 sampling cells in each field; (d) Final stage of learning using 80 cells; (e) Intermediate stage using 160 cells; (f) Final stage using 160 cells.

Figures 10.3b, d, and f illustrate the final, or asymptotic, LTM values that are obtained after many learning trials. Figures 10.3a, c, and e illustrate intermediate stages of learning. Figure 10.3a describes an intermediate LTM pattern prior to the final LTM pattern in Figure 10.3b. Using the pattern of final LTM values in Figure 10.3b as initial LTM values, an expanded field of sampling inputs then began to learn. Figure 10.3c shows a learning stage intermediate between Figures 10.3b and 10.3d. Then the field of sampling inputs was expanded again. Figure 10.3e shows a learning stage intermediate between Figures 10.3d and 10.3f. One can clearly see how new parts of the LTM maps build up in Figures 10.3a, c, and f.

We now quantify how well the map learning process in Figure 10.3 satisfies the properties of map invariance and self-regulation. Let m equal the number of sampling cells in each of the maps RM and EPM_1. In the following simulations, we chose $m = 40$, 80, and 160. In order to assess map invariance, we first define the mean values of all the LTM traces which abut each sampled cell in EPM_2. We compare these mean values with the sampled input patterns and with each LTM combination that corresponds to the same target position.

Thus we let

$$M_{k1}^{(m)} = \frac{1}{c(k)} \sum_{i+j=k} (z_{i1}^{(1)} + z_{j1}^{(2)}) \tag{10.31}$$

and

$$M_{k2}^{(m)} = \frac{1}{c(k)} \sum_{i+j=k} (z_{i2}^{(1)} + z_{j2}^{(2)}). \tag{10.32}$$

where $c(k)$ is the number of combinations of i and j such that $i + j = k$. In particular,

$$c(k) = \begin{cases} k-1 & \text{if } k = 2, 3, \ldots, m \\ 2m-k+1 & \text{if } k = m+1, m+2, \ldots, 2m. \end{cases} \tag{10.33}$$

Each summand in (10.31) equals the total LTM trace $z_{i1}^{(1)} + z_{j1}^{(2)}$ from $v_i^{(1)}$ in RM and $v_j^{(2)}$ in EPM_1 such that $i + j = k$. If RM and EPM_1 can cooperate to learn the EPM_2 patterns, then after sufficiently many learning trials, each summand $z_{i1}^{(1)} + z_{j1}^{(2)}$ in (10.31) should approximate $I_1 = K - L(i+j)$, by (10.29) and (10.30), and each summand $z_{i2}^{(1)} + z_{j2}^{(2)}$ in (10.32) should approximate $I_2 = L(i+j)$, by (10.30), for all i and j such that $i + j = k$. Consequently the following standard deviations should be small.

Invariant Map

Let

$$U_k^{(m)} = \left[\sum_{i+j=k} \left[(z_{i1}^{(1)} + z_{j1}^{(2)} - M_{k1}^{(m)})^2 + (z_{i2}^{(1)} + z_{j2}^{(2)} - M_{k2}^{(m)})^2 \right] \right]^{\frac{1}{2}} \tag{10.34}$$

$$V_k^{(m)} = \left[\left(\frac{M_{k1}^{(m)}}{M_k^{(m)}} - \frac{K - Lk}{K}\right)^2 + \left(\frac{M_{k2}^{(m)}}{M_k^{(m)}} - \frac{Lk}{K}\right)^2\right]^{\frac{1}{2}} \tag{10.35}$$

where

$$M_k^{(m)} = M_{k1}^{(m)} + M_{k2}^{(m)}. \tag{10.36}$$

Figures 10.4 and 10.5 show that both standard deviations are small for each choice of $m = 40$, 80, 160 and all k within the chosen range. The standard deviations $U_k^{(m)}$ in (10.34) show that each combination of retinal position and eye position comes close to the mean value corresponding to the target position. This measure shows that the map exhibits invariance, but it does not show that this invariant map actually learns the input pattern. The standard deviations $V_k^{(m)}$ in (10.35) show that the mean values corresponding to different target positions do learn the input patterns which they sample, up to a scaling factor.

To establish map self-regulation, we must show that the LTM maps are insensitive to the size m of the sampling sets in RM and EPM_1. Our computer simulations using the following standard deviations establish this property.

Self-Regulating Map

The numbers

$$W_k^{(M,m)} = \left[(M_{k1}^{(M)} - M_{k1}^{(m)})^2 + (M_{k2}^{(M)} - M_{k2}^{(m)})^2\right]^{\frac{1}{2}} \tag{10.37}$$

should be small for every pair of sampling set sizes m and M such that $M > m$ and $k = 2, 3, \ldots, 2m$. In Figure 10.6 we plot $W_k^{(M,m)}$ where $m = 40$ and $M = 80$ or 160. The small values of $W_k^{(M,m)}$ demonstrate map self-regulation.

Figure 10.7 illustrates that the map learning process is just as effective if the initial LTM values are randomly chosen numbers between 0 and 1, rather than the zero initial LTM values of Figure 10.3a. Again similar LTM maps emerge. These figures thus show the stability with which the LTM traces form invariant self-regulating asymptotic LTM patterns.

The numerical parameters used to generate Figures 10.3–10.7 are listed below for completeness. The learning rate parameter ϵ in (10.25) and (10.26) was chosen so small that the potentials x_1 and x_2 in (10.21) and (10.23) were always in an approximate equilibrium with respect to the inputs and LTM traces. Hence we set $\frac{d}{dt}x_1 = \frac{d}{dt}x_2 = 0$ and substituted the equations

$$x_1 = I_1 + z_1 \tag{10.38}$$

$$x_2 = I_2 + z_2 \tag{10.39}$$

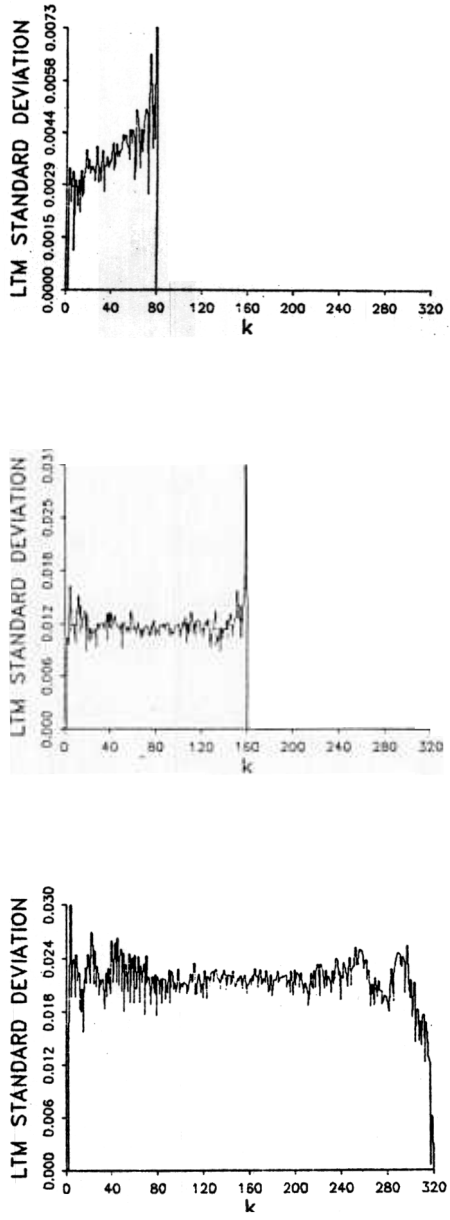

Figure 10.4. Standard deviation $U_k^{(m)}$ in equation (10.34) which measures map invariance: Each picture plots $U_k^{(m)}$ as a function of k with a different value of $m = 40$, 80, or 160.

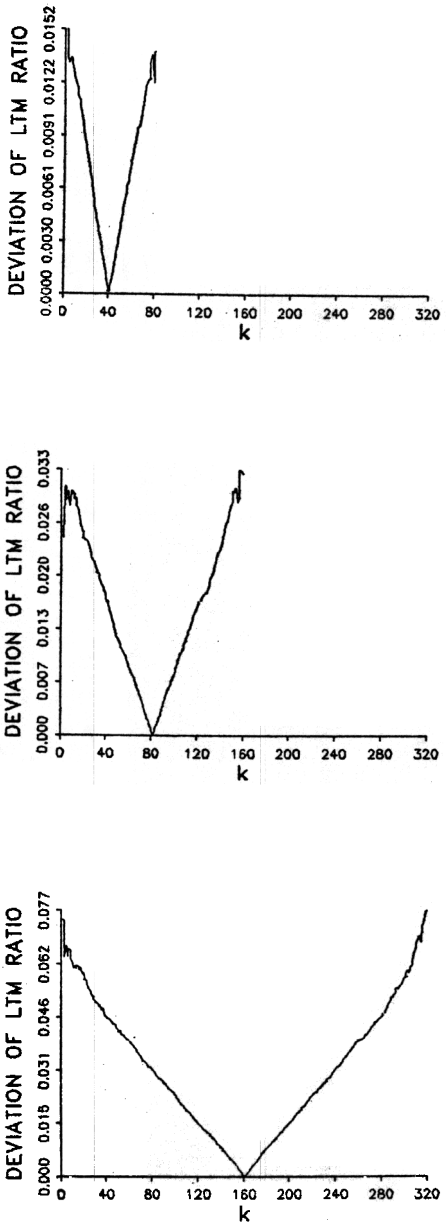

Figure 10.5. Standard deviation $V_k^{(m)}$ in equation (10.35) which measures map invariance: Each picture plots $V_k^{(m)}$ as a function of k with a different value of $m = 40$, 80, or 160.

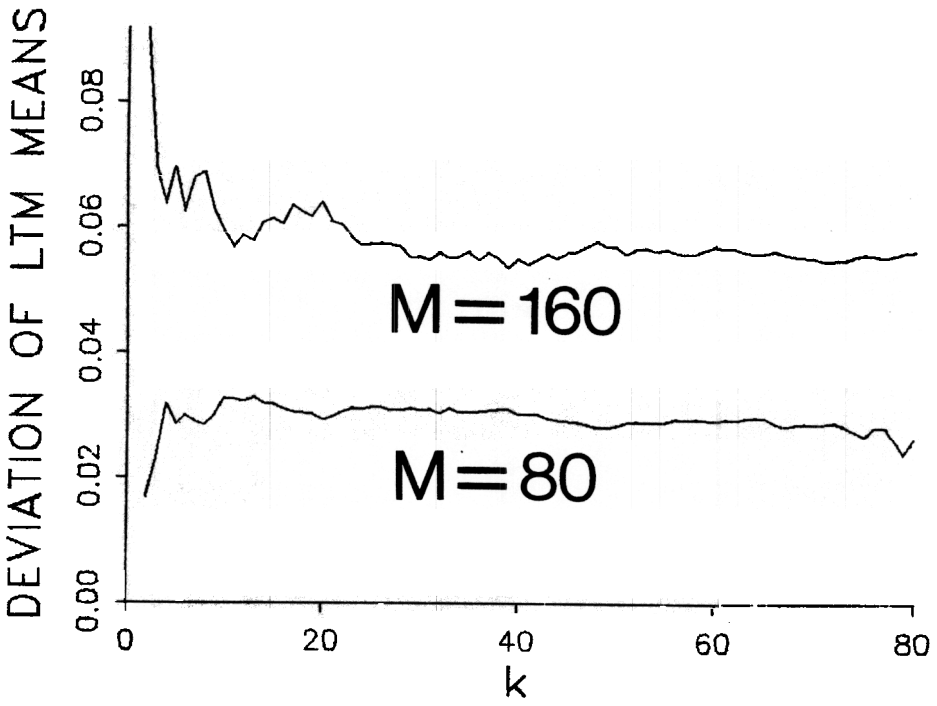

Figure 10.6. Standard deviation $W_k^{(M,40)}$ in equation (10.36) which measures map self-regulation: Each picture plots $W_k^{(M,40)}$ as a function of k with $M = 80$ or 160.

into the LTM equations (10.25) and (10.26). In these LTM equations, we chose

$$F = .2, \tag{10.40}$$

$$G = 1, \tag{10.41}$$

$$H = 2. \tag{10.42}$$

We also chose

$$p = q = 160 \tag{10.43}$$

as the total number of sampling cells in RM and in EPM_1. In the input functions (10.29) and (10.30), we let

$$L = \frac{2}{p+q} = \frac{1}{160} \tag{10.44}$$

and

$$M = 2(1+L) = \frac{161}{80}. \tag{10.45}$$

Consequently input I_1 in (10.29) varied from $\frac{1}{160}$ to 2 and input I_2 in (10.30) varied from 2 to $\frac{1}{160}$ across learning trials. The total number of learning trials used in Figure 10.3 was $5(10)^5$, divided among the $(160)^2$ possible combinations of randomly chosen sampling pairs. For initial conditions, we chose $x_1(0) = x_2(0) = 0$. We also chose all initial LTM traces equal to zero (Figure 10.3) or equal to randomly chosen numbers between 0 and 1 (Figure 10.7).

10.7. Multimodal Learning of an Invariant Self-Regulating Target Position Map

In order to study formation of a topographic TPM, we replaced the two population EPM_2 of the preceding example with a multicellular EPM_2 network. In order to achieve manageable computation times, we let RM, EPM_1, and EPM_2 each have 40 cells, or cell populations. The activity of the kth cell in EPM_2 was defined by

$$\frac{d}{dt}x_k = -x_k + I_k + z_k, \tag{10.46}$$

$k = 1, 2, \ldots, r$, where

$$z_k = \sum_{i=1}^{p} S_i^{(1)} z_{ik}^{(1)} + \sum_{j=1}^{q} S_j^{(2)} z_{jk}^{(2)}. \tag{10.47}$$

The LTM equations for $z_{ik}^{(1)}$ and $z_{jk}^{(2)}$ are the same as in (10.25) and (10.26) with the addition that $i = 1, 2, \ldots, p$, $j = 1, 2, \ldots, q$, and $k = 1, 2, \ldots, r$.

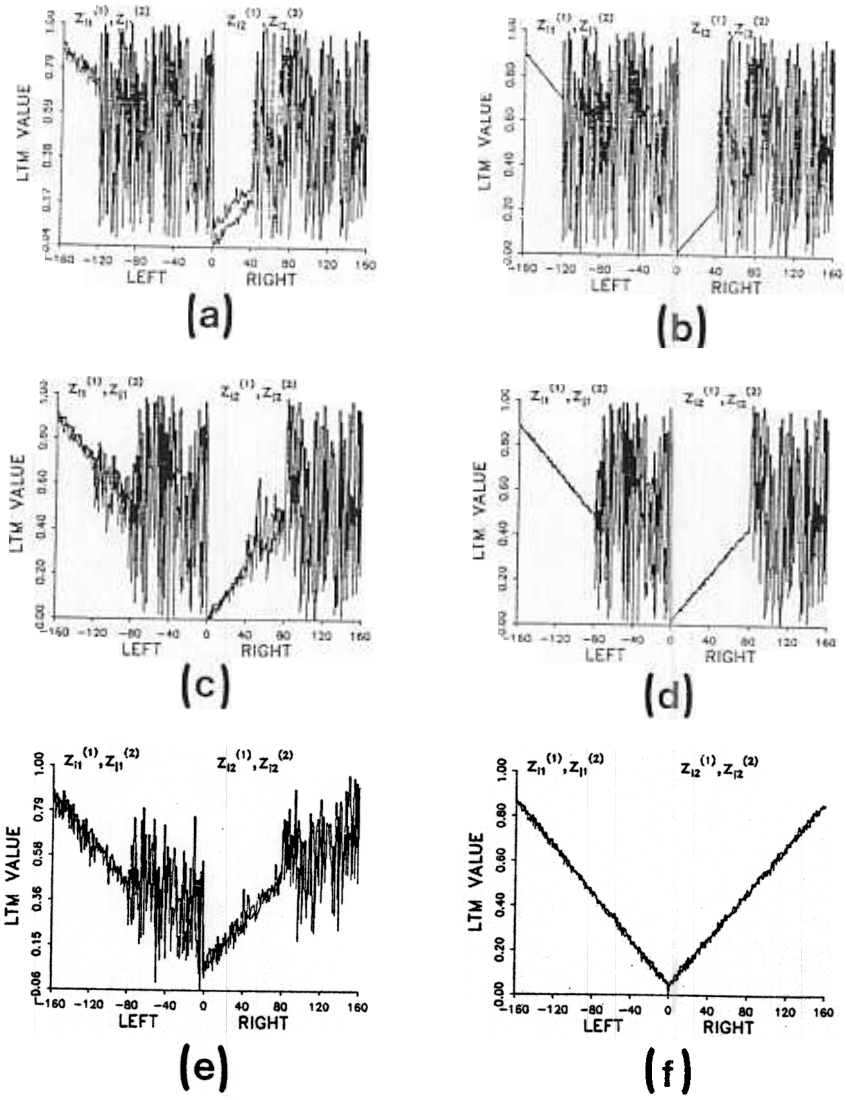

Figure 10.7. Expansion of LTM maps due to increase of the number of cells in the RM and the EPM_1 which sample the EPM_2: Initial LTM values are chosen randomly between 0 and 1 instead of equal to zero, as in Figure 10.3. The final learned LTM values in Figure 10.3 and this figure agree, thereby illustrating the stability of this invariant self-regulating map learning process.

In our simulations, $p = q = r = 40$. The main difference between this example and the previous one is that here the EPM_2 represented target eye positions by spatially focussed peaks. To represent this spatial map, we defined i_n and j_n as before, let

$$k_n = \left[\left| \frac{(i_n + j_n)r}{p+q} \right|\right] \tag{10.48}$$

and chose the input to cell v_k in EPM_2 on trial n to equal

$$I_{kn} = e^{\frac{-(k-k_n)^2}{\lambda}} \tag{10.49}$$

where $[\| w \|]$ denotes the largest integer less than or equal to w. Equation (10.49) says that the maximal activation of EPM_2 on trial n occurs at position $k = k_n$. Other activations of EPM_2 on trial n are Gaussianly distributed around position $k = k_n$. Position k_n represents the target position attained by the nth saccade. In (10.48), we scaled k_n using the factor $r(p+q)^{-1}$ to keep it between 1 and the number of cells r within the EPM_2.

Figure 10.8 plots the LTM surfaces generated by this learning model. As before, invariant map learning was excellent. We quantified how well an invariant map was learned as follows. After the $5(10)^5$ learning trials were over, we fixed the LTM values. We then randomly chose 10,000 combinations of cells in the RM, the EPM_1, and the EPM_2. As before, we let $i = i_n$ be the index of the RM population and $j = j_n$ be the index of the EPM_1 population on the nth choice. In addition, we let $k = m_n$ be the index of the EPM_2 population on the nth choice. In terms of these choices, we compared the relative sizes of LTM traces and inputs on the nth random choice using the function

$$Y_n = \left| \frac{z^{(1)}_{i_n m_n} + z^{(2)}_{i_n m_n}}{Z^{(n)}} - \frac{I_{m_n n}}{I^{(n)}} \right|, \tag{10.50}$$

where

$$Z^{(n)} = \sum_{k=1}^{40} (z^{(1)}_{i_n k} + z^{(2)}_{j_n k}), \tag{10.51}$$

$$I^{(n)} = \sum_{k=1}^{40} I_{m_n k}, \tag{10.52}$$

$$I_{m_n k} = e^{\frac{-(m_n - k_n)^2}{\lambda}}, \tag{10.53}$$

and k_n is defined in terms of i_n and j_n by (10.48). Then we computed the average size of the values Y_n in terms of the function

$$Y = \frac{1}{10,000} \sum_{n=1}^{10,000} Y_n. \tag{10.54}$$

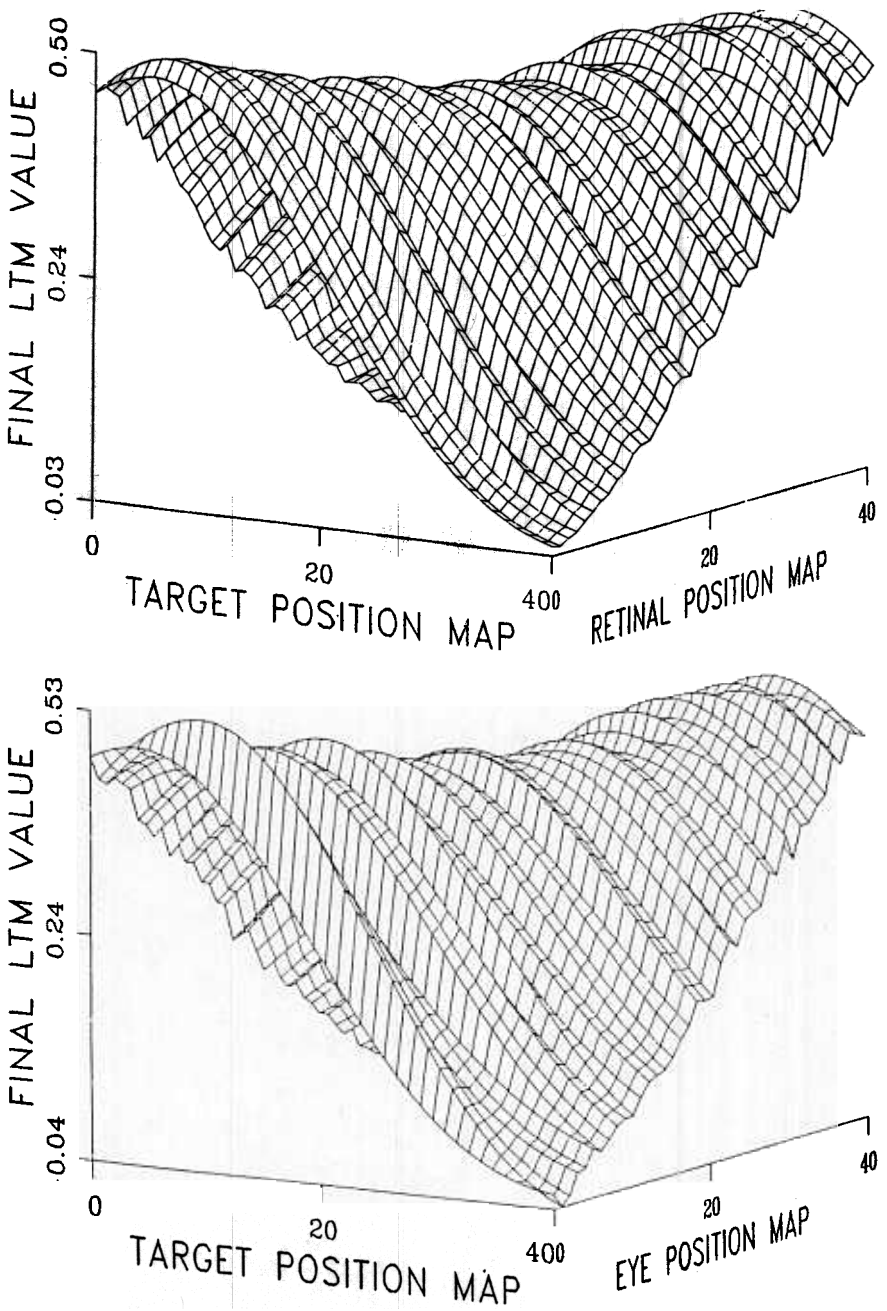

Figure 10.8. Final LTM values when randomly chosen RM and EPM_1 positions sample activity gradients distributed as Gaussians across a spatial topography defined in equation (10.49): The graphs depict the spatial distributions of LTM values across EPM_2 corresponding to each RM and EPM_1 position.

In our simulations, $Y = .0515$. Since the LTM traces and inputs varied between 0 and 1, this error represents excellent learning of the invariant map.

10.8. Associative Pattern Learning

Some mathematical insight can be gleaned into how multimodal map learning occurs by noticing that system (10.21)–(10.26) has the properties of a completely nonrecurrent associative learning network (Grossberg, 1969c, 1972b, 1982a). The stable pattern learning properties of these networks also hold in the present case. These properties enable one to understand how the correct *relative* LTM pattern values are learned by each sampling cell. The correct self-regulating *absolute* LTM values are learned due to the action of the autoreceptors.

In order to clarify these associative learning properties, we define two types of variables.

Total Activity Variables

Let

$$I = I_1 + I_2, \tag{10.55}$$

$$x = x_1 + x_2, \tag{10.56}$$

$$z_{ij1} = z_{i1}^{(1)} + z_{j1}^{(2)}, \tag{10.57}$$

$$z_{ij2} = z_{i2}^{(1)} + z_{j2}^{(2)}, \tag{10.58}$$

and

$$z_{ij} = z_{ij1} + z_{ij2}. \tag{10.59}$$

Relative Activity Variables

Let

$$\theta_1 = \frac{I_1}{I}, \tag{10.60}$$

$$\theta_2 = \frac{I_2}{I}, \tag{10.61}$$

$$X_1 = \frac{x_1}{x}, \tag{10.62}$$

$$X_2 = \frac{x_2}{x}, \tag{10.63}$$

$$Z_{ij1} = \frac{z_{ij1}}{z_{ij}}, \tag{10.64}$$

and

$$Z_{ij2} = \frac{z_{ij2}}{z_{ij}}. \tag{10.65}$$

Our goal is to indicate how relative pattern learning occurs. On a trial when $v_i^{(1)}$ is active in RM and $v_j^{(2)}$ is active in EPM_1, the relative LTM traces Z_{ij1} and Z_{ij2} in (10.64) and (10.65) measure how well RM and EPM_1 have cooperated to learn the relative inputs θ_1 and θ_2 in (10.60) and (10.61). We will show that the relative LTM pattern (Z_{ij1}, Z_{ij2}) is attracted to the relative input pattern (θ_1, θ_2) via the relative STM pattern (X_1, X_2) of (10.62) and (10.63).

On a learning trial when $v_i^{(1)}$ and $v_j^{(2)}$ are active, z_1 in (10.22) and z_2 in (10.24) reduce to

$$z_1 = z_{ij1} \tag{10.66}$$

$$z_2 = z_{ij2}, \tag{10.67}$$

where z_{ij1} and z_{ij2} are defined in (10.57) and (10.58), respectively. Consequently, (10.21) and (10.23) reduce to

$$\frac{d}{dt}x_1 = -x_1 + I_1 + z_{ij1} \tag{10.68}$$

and

$$\frac{d}{dt}x_2 = -x_2 + I_2 + z_{ij2}. \tag{10.69}$$

Adding (10.68) and (10.69) implies that

$$\frac{d}{dt}x = -x + I + z_{ij}. \tag{10.70}$$

For similar reasons on such a learning trial, addition of (10.25) and (10.26) implies that

$$\frac{d}{dt}z_{ij1} = e[-(F + 2H)z_{ij1} + 2Gx_1] \tag{10.71}$$

and

$$\frac{d}{dt}z_{ij2} = e[-(F + 2H)z_{ij2} + 2Gx_2], \tag{10.72}$$

from which it follows by a further addition of (10.71) and (10.72) that

$$\frac{d}{dt}z_{ij} = e[-(F + 2H)z_{ij} + 2Gx]. \tag{10.73}$$

We use these equations to derive equations for the relative STM and LTM traces. The basic tool is the elementary formula for the derivative of a ratio:

$$\frac{d}{dt}\left(\frac{f}{g}\right) = \frac{1}{g}\left[f - \frac{f}{g}\frac{d}{dt}g\right)\Big], \tag{10.74}$$

which we apply to the ratios $X_1 = \frac{x_1}{x}$, $X_2 = \frac{x_2}{x}$, $Z_{ij1} = \frac{z_{ij1}}{z_{ij}}$, and $Z_{ij2} = \frac{z_{ij2}}{z_{ij}}$. We find the familiar pattern learning equations

$$\frac{d}{dt}X_k = P_{ijk}(Z_{ijk} - X_k) + Q_k(\theta_k - X_k) \tag{10.75}$$

and

$$\frac{d}{dt}Z_{ijk} = R_{ijk}(X_k - Z_{ijk}), \tag{10.76}$$

$k = 1, 2$, where the coefficients are the nonnegative functions

$$P_{ijk} = \frac{z_{ij}}{x_k}, \tag{10.77}$$

$$Q_k = \frac{I}{x_k}, \tag{10.78}$$

and

$$R_{ijk} = \frac{2\epsilon G x}{z_{ijk}} \tag{10.79}$$

Term $Q_k(\theta_k - X_k)$ in (10.75) describes read-in of the input pattern θ_k into STM X_k. This term causes X_k to approach θ_k. Term $P_{ijk}(Z_{ijk} - X_k)$ describes read-out of LTM into STM. It causes X_k to approach Z_{ijk}. Thus the relative STM trace X_k is torn between the tendency to represent new, as yet unlearned, patterns θ_k and to read-out old remembered patterns Z_{ijk}. Term $R_{ijk}(X_k - Z_{ijk})$ in (10.76), on the other hand, describes read-in of STM into LTM. This term causes Z_{ijk} to approach X_k. In all, the STM and LTM patterns mutually attract each other, while the STM pattern is attracted to the input pattern:

$$Z_{ijk} \leftrightarrow X_k \rightarrow \theta_k. \tag{10.80}$$

The net effect of these attractive tendencies is that the LTM pattern is attracted towards the input pattern:

$$Z_{ijk} \rightarrow \theta_k. \tag{10.81}$$

This is true given any fixed but random choice of i and j through time. The simulations demonstrate that, in response to a randomly chosen sequence of (i, j) pairs through time, these learning tendencies fit together to synthesize a globally consistent, invariant, self-regulating TPM.

The role of autoreceptors in enabling the network to self-regulate is indicated by an examination of the LTM traces of equation (10.25) at equilibrium. At equilibrium, $\frac{d}{dt}x_1 = 0$. Then (10.21) becomes

$$x_1 = I_1 + z_1. \tag{10.82}$$

Consider $z_{i1}^{(1)}$ in (10.25) by letting $k = 1$. If we substitute for x_1 in this equation, we get

$$\frac{d}{dt}z_{i1}^{(1)} = \epsilon S_i^{(1)}\left[-Fz_{i1}^{(1)} + G(I_1 + z_1) - Hz_1\right]. \tag{10.83}$$

At equilibrium, $\frac{d}{dt}z_{i1}^{(1)} = 0$, which by (10.83) implies that

$$Fz_{i1}^{(1)} + (H - G)z_1 = GI_1. \tag{10.84}$$

We assume that the LTM decay rate F is very small. Then (10.84) implies that

$$z_1 \cong \frac{G}{H - G}I_1. \tag{10.85}$$

Thus the relative size of H to G determines the scaling factor that converts inputs into LTM values. This scaling factor does not influence the goodness-of-fit measured by $V_k^{(m)}$ in (10.35).

On the nth learning trial, $z_1 = z_{i_n1}^{(1)} + z_{j_n2}^{(2)}$ due to equations (10.27) and (10.28). Thus for all large choices of n, when the network is close to equilibrium, (10.85) implies

$$z_{i_n1}^{(1)} + z_{j_n2}^{(2)} \cong \frac{G}{H - G}I_1. \tag{10.86}$$

Given that the network can approach an approximate equilibrium as n becomes sufficiently large, equation (10.86) has the following implications. First, it implies that $H > G$. Computer simulations show that system variables can diverge if $H - G$ becomes too small. Second, equation (10.86) shows that the equilibrium value of each LTM trace $z_{i1}^{(1)}$ depends upon the equilibrium values of all LTM traces $z_{j2}^{(2)}$ with which it is paired. In particular, each $z_{i1}^{(1)}$ adjusts its equilibrium value to compensate for the addition or deletion of LTM values $z_{j2}^{(2)}$, as in Figure 10.3. Thus equation (10.86) describes a sharing of adaptive load quite different from that described in Chapter 3. The present type of load sharing is the property of self-regulation that we seek. The problem remains open of mathematically proving that this nonlinear system of stochastic differential equations always approaches an approximate equilibrium as $n \to \infty$ if $H - G$ is sufficiently large, ϵ is sufficiently small, and the input indices i_n and j_n are randomly chosen.